ACCOUNTS
of chemical research

Synthesis of Soluble Graphite and Graphene

K. F. KELLY[‡] AND W. E. BILLUPS[*,†]

[†]*Department of Chemistry and The Richard E. Smalley Institute for Nanoscale Science and Technology, Rice University, 6100 Main Street, Houston, Texas, 77005, United States, and* [‡]*Department of Electrical and Computer Engineering and the Rice Quantum Institute, Rice University, 6100 Main Street, Houston, Texas, 77005, United States*

RECEIVED ON APRIL 28, 2012

CONSPECTUS

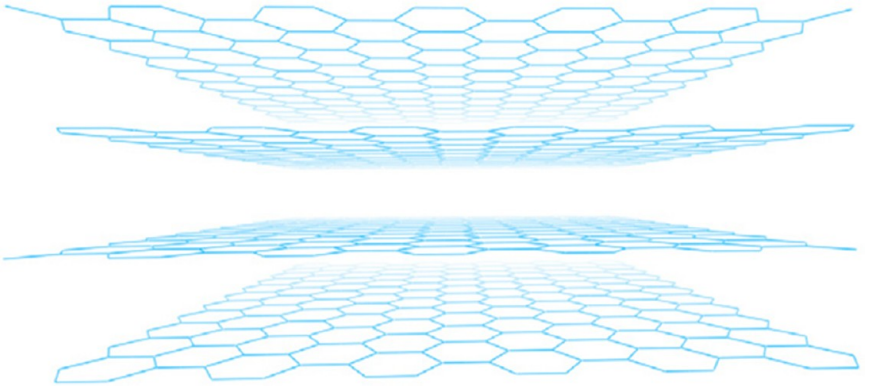

Because of graphene's anticipated applications in electronics and its thermal, mechanical, and optical properties, many scientists and engineers are interested in this material. Graphene is an isolated layer of the π-stacked hexagonal allotrope of carbon known as graphite. The interlayer cohesive energy of graphite, or exfoliation energy, that results from van der Waals attractions over the interlayer spacing distance of 3.34 Å (61 meV/C atom) is many times weaker than the intralayer covalent bonding. Since graphene itself does not occur naturally, scientists and engineers are still learning how to isolate and manipulate individual layers of graphene. Some researchers have relied on the physical separation of the sheets, a process that can sometimes be as simple as peeling of sheets from crystalline graphite using Scotch tape. Other researchers have taken an ensemble approach, where they exploit the chemical conversion of graphite to the individual layers. The typical intermediary state is graphite oxide, which is often produced using strong oxidants under acidic conditions. Structurally, researchers hypothesize that acidic functional groups functionalize the oxidized material at the edges and a network of epoxy groups cover the sp^2-bonded carbon network. The exfoliated material formed under these conditions can be used to form dispersions that are usually unstable. However, more importantly, irreversible defects form in the basal plane during oxidation and remain even after reduction of graphite oxide back to graphene-like material.

As part of our interest in the dissolution of carbon nanomaterials, we have explored the derivatization of graphite following the same procedures that preserve the sp^2 bonding and the associated unique physical and electronic properties in the chemical processing of single-walled carbon nanotubes. In this Account, we describe efficient routes to exfoliate graphite either into graphitic nanoparticles or into graphene without resorting to oxidation. Our exfoliation process involves the intercalation of lithium into bulk graphite to yield graphene sheets reduced by the lithium. We can alkylate the resulting graphite salt reductively using solubilizing dodecyl groups. By probe microscopy, we show that these groups are attached covalently only at the graphitic edges.

1. Introduction

Graphene occupies a central position among the group of carbon nanomaterials that are poised to occupy a significant role in nanoscience and nanotechnology.[1−23] Graphene is defined as individual or few-layer stacked sheets of sp^2-hybridized carbon where the number of sheets does not exceed 10.[24] Beyond a single layer, it occurs in a stacked hexagonal structure of graphite with an interlayer spacing of 3.34 Å, the van der Waals distance for sp^2-bonded carbon. The interlayer cohesive energy or exfoliation

Published on the Web 11/01/2012 www.pubs.acs.org/accounts
10.1021/ar300121q © 2012 American Chemical Society

energy for pyrolytic graphite has been determined experimentally as 61 meV/C atom.[5,25] A 1 nm square of graphene contains about 38 carbon atoms, and the separation energy of two 1 nm squares of graphene is greater than 2 eV.[25] Graphene itself does not occur naturally (although graphite does), and prior work has relied on the physical separation of the sheets under special conditions. The efficient exfoliation of precursor materials is thus a major barrier in the synthesis of soluble graphene.

Exfoliation has been achieved by either physical peeling the top surface of pyrolytic graphite[26] or by chemical exfoliation of the oxidation products of graphite (graphite oxide).[27−29] Various reagents have been used to remove the oxygen functionality from graphite oxide. Typical reducing agents are hydrazine and dihydrogen. Under these conditions, the original crystalline structure of the graphene basal plane is not completely restored as the graphene oxide is heavily functionalized by chemical defects, such as holes, that are introduced. These subsequent defects are not readily healed, even upon annealing.

The use of intercalating agents[30−33] provides an attractive way to exfoliate graphite while preserving the unique properties of a continuous graphene sheet. Graphite intercalation compounds are formed by the insertion of atomic or molecular layers of a chemical species called the intercalant between the layers of a graphite host material. These intercalants are commonly classified according to whether they form donor or acceptor compounds.[34] The most common and most widely studied of the donor compounds are the alkali metal compounds Li, K, Rb, and Cs.[34] As part of our interest in the dissolution of carbon nanomaterials, we have explored the derivatization of graphite, following procedures that we developed previously for the chemical processing of single-walled carbon nanotubes.[35] In this Account, we describe the variety of conditions that we have used to functionalize graphene by the addition of solubilizing groups. In addition to thorough chemical characterization, we also performed nanoscale characterization with scanning probe microscopy to demonstrate purely edge functionalization by such reactions.

2. Exfoliated Soluble Graphite

Our early studies were carried out with partially exfoliated commercial graphite[36] that was obtained as a dark gray hydrophobic powder. Functionalization reactions were achieved by adding lithium to a dispersion of the graphite in liquid ammonia as illustrated in Scheme 1.

SCHEME 1. Functionalization of Graphite by Dodecyl Radicals

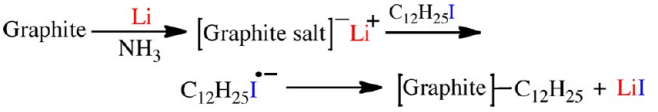

The intercalation of lithium[34] into the graphite leads to negatively charged sheets of graphene that serve as a source of electrons to form the dodecyl iodide radical anion. The radical anion provides dodecyl radicals that form covalent bonds to the graphene. Dodecyl radicals formed via this strategy add readily to other carbon nanomaterials[35,37,38] and serve as excellent solubilizing groups.

Covalent attachment of the dodecyl radicals to the graphite can be demonstrated by Raman spectroscopy where the *D* band observed at 1299 cm^{-1} is substantially enhanced as a result of the chemical disruption of the sp^2 hybridized carbon atoms of the graphite. A weight loss of 24% was determined by thermogravimetric analysis (TGA), indicating that one dodecyl group is present for every 40 graphitic carbon atoms. No significant increase in the

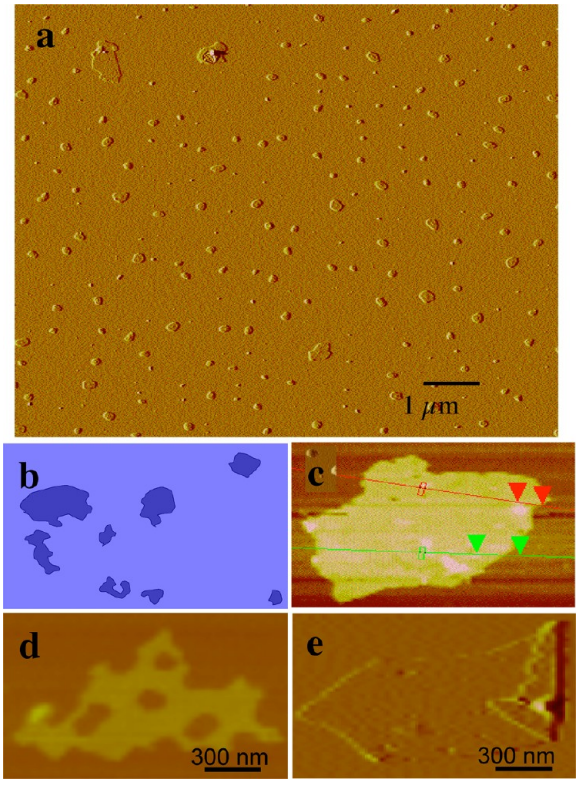

FIGURE 1. (a) AFM image showing different shapes of dodecylated graphite nanoplatelets after spin coating onto mica from chloroform. (b) Schematic representation of different shapes of a few layers of graphite found by optical microscopy. (c, d, e) Different shapes of dodecylated graphite structure found by AFM analyses. All images are reprinted from ref 36 with permission from Elsevier.

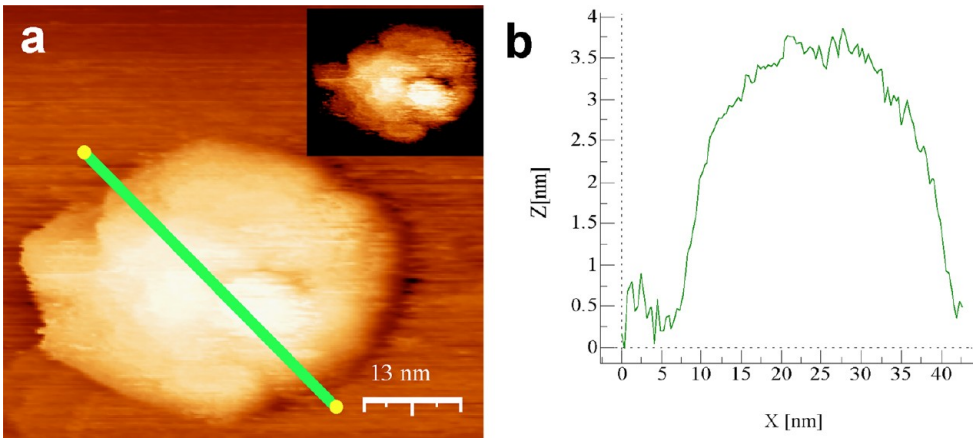

FIGURE 2. (a) STM image of dodecylated graphite nanoplatelets on Au(111) surface; bias voltage [V_b] = −0.1 V; tunneling current [I_t] = 0.1 nA. The bright feature shows multiple layers of graphene, and the inset is the high-pass filtered image. (b) Cross section of dodecylated graphite. Reprinted from ref 36 with permission from Elsevier.

D band was observed upon exposure of the graphite to lithium in liquid ammonia (without the iodide).

The sheet resistivity of the unfunctionalized graphite, dodecylated graphite, and the material obtained after thermolysis was measured. The resistivity of the dodecylated graphite (8.3×10^{-3} Ω cm) is, as expected, greater than that of the starting material (2.1×10^{-3} Ω cm). This increase is due to interruption of the graphite network by the covalently bound dodecyl groups. A small increase of resistivity (5.7×10^{-3} Ω cm) is observed after thermal removal of the dodecyl groups, probably the result of defects created by this process.

To characterize the soluble species by atomic force microscopy (AFM), solutions were spin coated onto mica from chloroform as shown in Figure 1a. The irregular, ragged shapes of the nanoplatelets may reflect the conditions used to prepare the graphite that served as the starting material.[36]

More detailed images of the irregular graphite nanoplatelets are shown in Figure 1b−e. The horizontal distance of these sheets varies from 0.3 to 1.1 μm with a height of ∼3.5 nm (±0.2). Images with large holes (Figure 1c) and folded edges (Figure 1c) were observed in several instances. We have also used polarized light microscopy to image the dispersions of dodecylated graphite (Figure 1b).

Scanning tunneling microscopy (STM) was employed to accurately determine the height of the soluble graphite nanoplatelets and to provide direct information about the chemically modified surfaces. STM is an extremely useful tool for the determination of the surface coverage of functional groups and for visualization of the effect of functionalization. An STM image and cross section of the dodecylated graphite nanoplatelets are presented in Figure 2a and b, respectively. The height can be measured as 3.5 nm, corresponding to approximately 10 layers of graphene. By high-pass filtering of the original image, we could observe that the top surface consists of a few small graphene domains separated by single steps. We assume that the van der Waals forces are simply too strong to allow full exfoliation. It is interesting, however, that we are able to achieve nearly complete debundling of carbon nanotubes under similar conditions.[35]

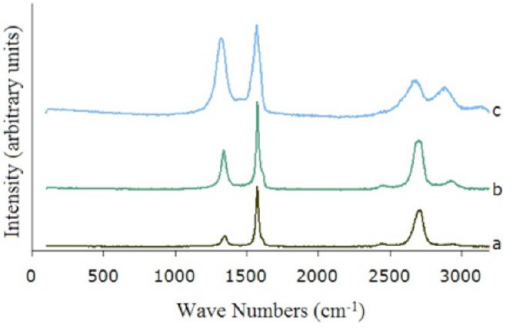

FIGURE 3. Raman spectra of (a) raw graphite, (b) graphite functionalized one time by dodecyl groups, and (c) graphite functionalized three times by dodecyl groups.

Powder X-ray diffraction (XRD) was used to determine the bulk property of the functionalized material. The XRD pattern of the starting material exhibits peaks corresponding to planes (002) and (004) located at 26.56° and 54.64°, respectively. The main peak (002) of dodecylated graphite is broader and lower in intensity than the starting material. Moreover, a small shift in the (002) peak position at 25.79° illustrates larger interplanar *d* spacing of the dodecylated material compared to the graphite. This is probably due to attachment of the dodecyl groups to the surface of the graphite.

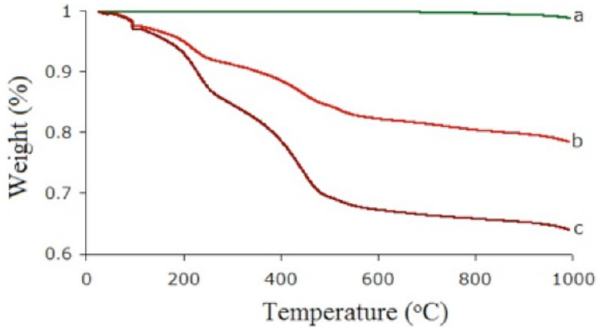

FIGURE 4. TGA of graphite: (a) raw graphite, (b) graphite functionalized one time by dodecyl groups, and (c) graphite functionalized three times by dodecyl groups.

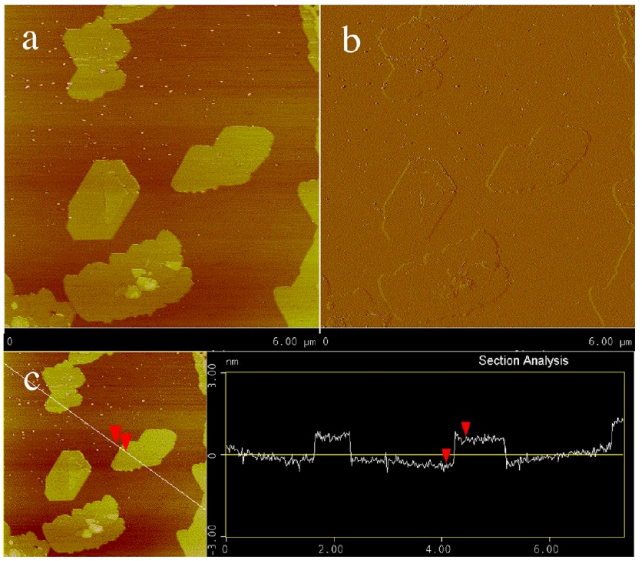

FIGURE 5. Tapping mode AFM images of dodecylated graphene (6 μm $\times$ 6 μm): (a) amplitude image showing topography of free-standing functionalized graphene; (b) is identical to (a) but expresses the *Z*-height in voltage; (c) corresponding section analysis (*x*-axis in μm and *y*-axis in nm), showing the height of dodecylated graphene is 0.8 to 1.0 nm and a diameter of ~1.0 to ~2.0 μm.

After subtracting the instrumental peak broadening using an NIST LaB_6 standard, the crystallite size is calculated from the residual peak broadening for (002) and (004) plane. The crystallite size is found to be ~19 nm for the commercial graphite and ~3.5 nm (±0.2) for dodecylated material, confirming the AFM and STM results. A glassy hump observed in the 14−40° range in the diffraction pattern indicates a reduction (~55%) in the crystallinity of the dodecylated material compared to the starting material.

Similar experiments were carried with other samples of graphite.[39] A high level of exfoliation could be obtained when Sigma Aldrich 282863 was reductively alkylated by dodecyl groups. Raman spectra are illustrated in Figure 3 where the functionalization scheme was carried out

SCHEME 2. Functionalization of Fluorinated Graphite by Dodecyl Radicals

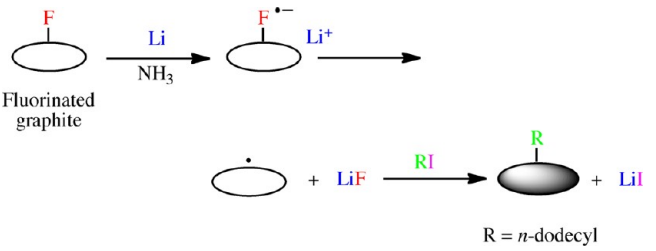

once (Figure 3, spectrum b) followed by functionalization of the same sample two additional times (Figure 3, spectrum c).

As seen in Figure 4, thermogravimetric analysis mirrors the Raman spectra. Whereas the raw graphite shows only a 1.0% weight lost on heating to 1000 °C, the more highly functionalized product exhibits a 33% weight loss after heating to 1000 °C. This corresponds to about one functional group per 49 carbon atoms.

The AFM images of the more highly functionalized graphene are presented in Figure 5.

3. Soluble Graphite Nanoplatelets from Graphite Fluoride

Soluble graphene layers can be formed when fluorinated graphite[40,41] is reacted with either alkyl lithium reagents[42] or is reductively alkylated by dodecyl groups.[43] Haddon and his co-workers prepared soluble graphene layers in a one-step synthesis by reacting graphite fluoride of various stoichiometries with *n*-butyl or *n*-hexyl lithium. As expected, the graphene functionalized by hexyl groups was more soluble than the butylayed products. Dealkylation was observed to occur upon annealing the bulk samples, thus restoring the electronic properties of graphene.

We succeeded in preparing highly functionalized graphitic nanoparticles by reductive alkylation of fluorinated graphite (C_1F_1)[43] as illustrated in Scheme 2. In accordance with the earlier studies,[40] the fluorinated graphite used for this work exhibited strong IR-stretching absorptions between 1072 and 1342 cm^{-1}.

During the functionalization process the white fluorinated graphite turns black, indicating that dodecyl radicals have replaced the fluorine groups. Electron transfer from lithium to the fluorinated graphite would yield a transient radical anion that would decompose rapidly leaving an electron to reside on the graphene. Electron transfer to the dodecyl iodide would provide the dodecyl radicals that form a covalent bond to the graphene. A radical transfer

mechanism has been observed previously when fluorinated carbon nanotubes are alkylated reductively.[44]

The dodecylated graphite exhibits a prominent disorder mode (*D* band) at 1290 cm^{-1}. The *D*:*G* ratio is 2:1, indicating a high level of functionalization as shown in Figure 6. Similar results were reported by Haddon and co-workers for the material obtained from the reaction of fluorinated graphite with alkyl lithium reagents.[42] A *D*:*G* ratio of 1:1 has been reported for fluorinated carbon nanofibers.[45]

The TGA weight loss of the degassed dodecylated graphite is 40%, indicating that the functionalized material has 1 dodecyl group per 21 graphitic carbon atoms. This probably accounts for the high level of solubility in organic solvents including $CHCl_3$, CH_2Cl_2, DMF, DMSO, benzene, and 1,2,4-trichlorobenzene. The solubility in $CHCl_3$ was determined to be 1.2 g/L.

AFM images of the dodecylated graphite show irregular graphite nanoplatelets, an example of which is displayed in Figure 7. The horizontal distance varies between ~0.1 and 0.5 μm. The average height varies between ~2 and 12 nm with 50% of the functionalized platelets having a thickness of 8 nm, indicative of ~23 graphene sheets per nanoplatelet.

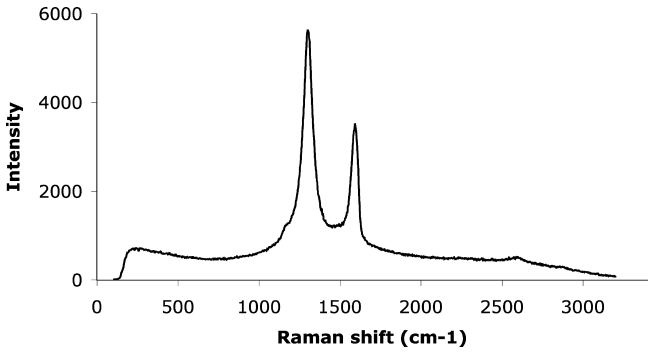

FIGURE 6. Raman spectrum (780 nm excitation) of dodecylated graphite.

X-ray photoelectron spectroscopy (XPS) provides direct evidence for replacement of the fluorine atoms by dodecyl groups. XPS spectra corresponding to the region between 0 and 1100 eV of the starting graphite fluoride showed only the presence of carbon and fluorine. The percentage of fluorine in the graphite fluoride obtained from XPS compares favorably with the earlier work[40] where the ratio was found to be (C_1F_1). Nearly all of the fluorine atoms are displaced by the dodecyl functionalities during the reductive alkylation.

4. Functionalization of Potassium Graphite

When potassium is melted over graphite under an atmosphere of argon, a lamellar compound is formed by intercalation of potassium atoms between the graphene sheets.[46−51] The most common stoichiometry for this pyrophoric bronze powder is C_8K.[52] Although many applications of this material have been reported,[54−75] it is somewhat surprising that C_8K had not been used as a substrate for the synthesis of soluble derivatives of graphite. Indeed, we found that C_8K can be used as a point of departure for the synthesis of derivatized graphite nanoplatelets[53] using the

SCHEME 3. Functionalization of Potassium Graphite by Dodecyl Radicals

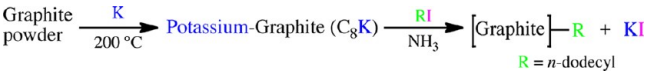

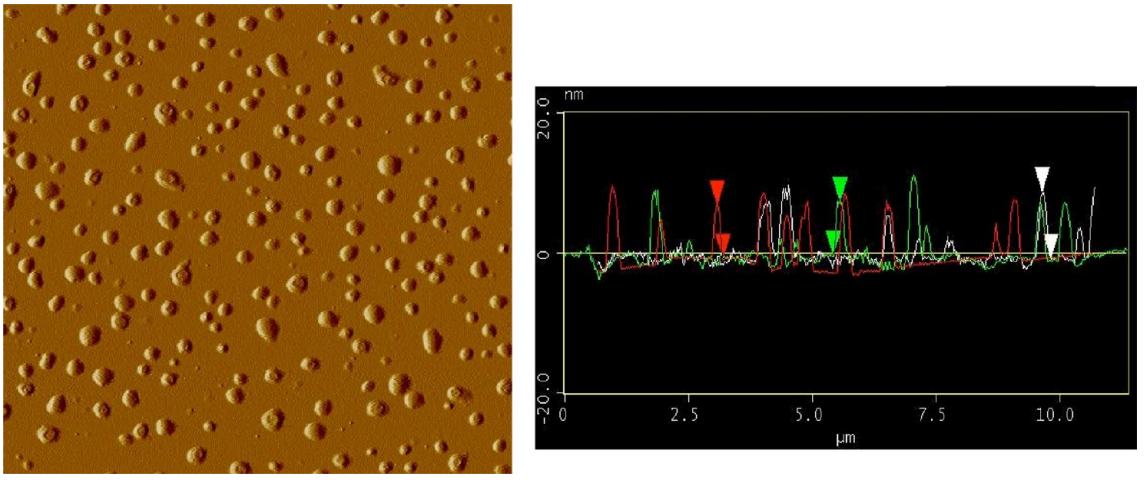

FIGURE 7. AFM (0 μm × 10 μm) amplitude image and section analysis (*x*-axis in μm and *y*-axis in nm) of dodecylated-graphite spin coated onto freshly cleaved mica from chloroform. Adapted from ref 43. Copyright 2008 American Chemical Society.

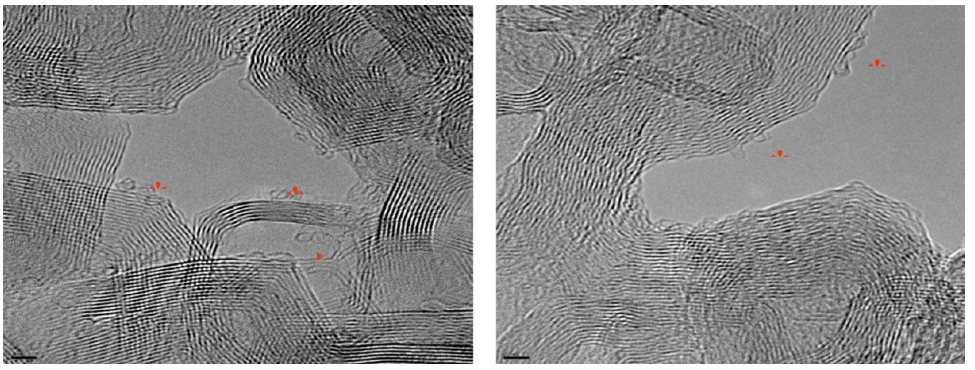

FIGURE 8. High resolution TEM images of water-soluble PEGylated graphite. Adapted from ref 53. Copyright 2007 Wiley.

SCHEME 4. Preparation of Water-Soluble PEGylated Graphite

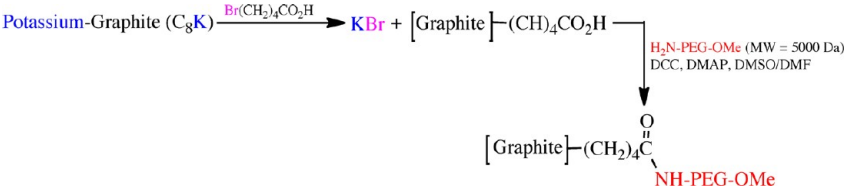

methodologies that have been described to functionalize other carbon nanomaterials.[35,76−78]

By treating freshly prepared C_8K with 1-iodododecane in liquid ammonia, a dodecylated graphitic product was formed (Scheme 3). This material was found to be soluble in several organic solvents including chloroform and 1,2,4-trichlorobenzene.

Thermogravimetric analyses gave a weight loss of 15%, corresponding to approximately one dodecyl group per 78 graphitic carbon atoms. A control experiment carried out with C_8K and ammonia led to a negligible increase in the intensity of the *D* band. Thus, the addition of hydrogen appears not to be a significant event.

The synthesis of a water-soluble product was achieved by initial functionalization of the graphite surface using 5-bromovaleric acid followed by PEGylation using amine-terminated poly(ethyleneglycol) (PEG) chains (Scheme 4). TGA analysis gave a weight loss corresponding to one $-(CH_2)_4CO_2H$ group per 61 graphitic carbons.

High-resolution transmission electron microscopy (TEM) images recorded for the PEGylated graphite show 6−20 layer-induced long fringes that have formed as tangled ribbons in a network-like structure as seen in Figure 8. Whereas TEM images of unfunctionalized graphite will have smooth sidewalls,[79] the "bumps" along the sidewalls of the graphitic structure are PEG groups,[78] emphasizing the propensity for edge functionalization. The particles have an average size of the order of 0.1 mm.

The average height distribution of the functionalized material determined by AFM is in good agreement with the layers observed in TEM images. The statistical distributions from 50 nanoplatelets show that 70% have an average height of 7−9 nm, whereas 30% have an average height of 2−4 nm. The horizontal distances across the nanoplatelets of these functionalized materials vary between 0.1−1.4 mm.

5. Water-Soluble Graphene

Water-soluble graphene can be prepared as illustrated in Scheme 5,[80] a route similar to that demonstrated earlier for carbon nanotubes[81] where highly cohesive van der Waals attractions[25] were overcome by sulfonation in oleum. Thus, addition of benzoyl peroxide to a suspension of graphite in benzene at 75−80 °C provides phenylated graphite that can be exfoliated and sulfonated concomitantly by treatment with oleum as illustrated in the scheme. The sodium sulfonate was prepared by adding 1 M sodium hydroxide to the exfoliated graphene. The salt was found to exhibit high solubility in water (2.1 mg/mL). As the following analysis will show, the functionalized exfoliated graphene is not only highly soluble thanks to attachment of the sodium sulfonate groups, but it is also relatively free of the basal plane defects that typically result from removal of the oxygen functionality of graphite oxide (GO) compounds.

Raman spectra are presented in Figure 9. The *D*, *G*, and 2*D* bands were recorded using 514.5 nm laser excitations. The starting graphite powder (Figure 10a) exhibits weak *D* and

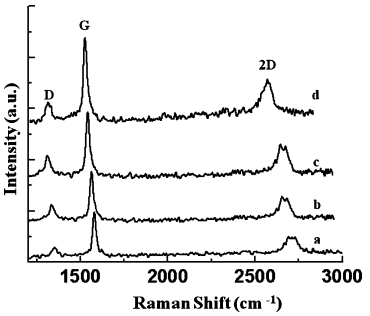

FIGURE 9. Raman spectra of (a) graphite, (b) phenylated graphite, (c) sulfonated graphene, and (d) sodium salt of sulfonated graphene.

2*D* bands that arise from defects. Functionalization of the graphitic edges might account for the weak enhancement of the *D* band. Sulfonation of the phenyl groups and the resulting repulsive interaction between the $—SO_3^{\delta-}$ groups leads to partial exfoliation as observed by the narrowing of the 2*D* peak. Finally, when the sodium salt is formed, a high degree of exfoliation is observed as demonstrated by the sharp 2*D* peak. This is attributed to charge repulsion of the SO_3^- groups.[82,83]

TGA analysis of the sulfonated graphene leads to a weight loss of 18%, indicating that one functional group is present for approximately 50 graphitic carbon atoms. This level of functionalization is consistent with the enhancement of the D band (Figure 9) and emphasizes the efficiency of the functionalization process.

To examine the atomic-scale structure, exfoliated graphene sheets of the sodium salt were deposited onto Au(111) substrates and imaged by scanning tunneling microscopy. The height of the graphitic nanostructures ranged from less than 2 and up to 5 nm, which corresponds to between 5 and 14 layers. Figure 10a and b corresponds to topographs from two such nanoparticles. Cross sections through each of these are displayed in Figure 10c, allowing the extrapolation of the number of layers. A high-pass filtered image of Figure 10b in panel (d) reveals the individual domains of the different layers.

Upon close inspection, clear atomic resolution was observed in several of the exfoliated sheets, one of which is shown in Figure 11a. Even at this scale, any defects on the terraces would be readily apparent in the STM images.[84] The corresponding height cross section displayed in Figure 11b shows clear quantized steps between these terraces that correspond well with expected interlayer spacing of bulk graphite. Figure 11c is a high-resolution image of the pristine atomic structure. Figure 11d is the corresponding 2-D Fourier transform of this image that further confirms the hexagonal

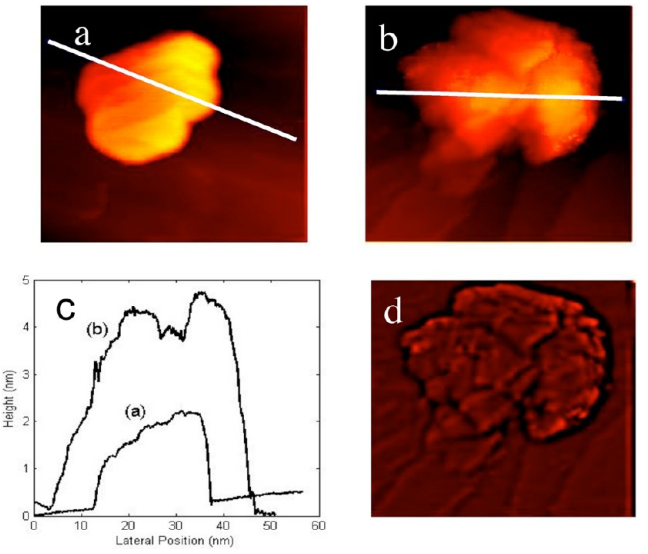

FIGURE 10. (a, b) STM images of exfoliated graphene on Au(111) substrates: (a) Image size: (57.6 × 57.6 nm^2), bias voltage [V_{bias}] = 100 mV, tunneling current [I_t] = 0.1 nA. (b) (56 × 56 nm^2), [V_{bias}] = −200 mV, [I_t] = 1 nA. (c) Cross sections of (a) and (b). (d) High-pass filtered image of (b) showing different domains and a single layer attached to multiple-layered structure. Adapted from ref 80. Copyright 2011 American Chemical Society.

graphitic lattice. This strongly supports the previous conclusion that the functionalization is performed on the dangling bonds at the edges without perturbing the sp^2 bonds of the basal plane. It also explains the weak *D* band appearance in the Raman spectra. The comparison of RMS edge roughness measurement of the exfoliated graphite to that of highly ordered bulk pyrolytic graphite shows higher roughness for the exfoliated graphite due to the functional groups on the edge. Under the same imaging conditions, the exfoliated graphene edges in Figure 11a show a 40% higher roughness compared to that of bulk graphite.

Stable solutions of the sodium salt in water are formed after sonication for a few minutes. These solutions remained stable for several months. The sheet resistance of bulk films prepared by vacuum filtration using an anodizc membrane (pore size ~ 20 nm) was determined using a four-point probe fitted to a custom built attachment with Pt leads for film testing. The sulfonated graphene (Scheme 5) gave an average value of 212 Ω/sq, while the starting graphite gave 960 Ω/sq. Thin film samples prepared from graphene oxide give a sheet resistance of about 1.8 kΩ/sq after annealing.[85,86] These measurements support our belief that chemical functionalization under these conditions preserves the crystalline structure of the graphene basal planes. Materials prepared from our water-soluble graphite will likely result in much higher conductivity than previous methods.

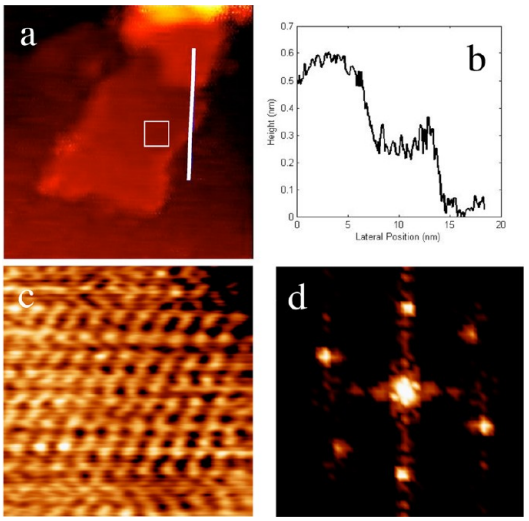

FIGURE 11. (a) Single layer of exfoliated graphene from lower left of (d) showing defects on the edges. Imaging conditions: 33.7 × 33.7 nm^2, $[V_{bias}] = -83$ mV, $[I_t] = 1.5$ nA. (b) Cross section of (a) showing normal layer spacing of graphite. (c) Atomic structure from the boxed area of (a). Imaging conditions: 3.6 × 3.6 nm^2, $[V_{bias}] = -83$ mV, $[I_t] = 2.3$ nA. (d) 2-D Fourier transform of (c). Adapted from ref 80. Copyright 2011 American Chemical Society.

SCHEME 5. Synthesis of Water-Soluble Graphene

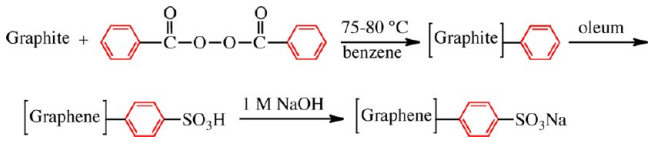

For comparison, the value reported for graphene grown on a nickel surface by Kim et al. is ~280 Ω/sq.[86]

6. Conclusions

While this Account includes only a small number of the many possible chemical methods for producing graphene nanoparticles from bulk graphite, the strategies presented here focus on synthetic routes that bypass an oxidative reaction of the material. The clear consequence of this is that much of the functionalization is limited to edges of the material and thus preserves the crystallinity of the basal plane where many of the unique electronic and mechanical properties of graphene are derived. This research is now at a stage where these compounds can be applied to various technologies, such as conductive coatings and carbon composites, where their performance can be directly compared with current materials.

The authors are deeply indebted to their past and current collaborators that have contributed to this work. Special thanks to Drs. Yanqiu Sun and Jianxin Lu for assistance with the manuscript. The authors received financial support for this research from the Robert A. Welch Foundation (C-0490 and C-1605), the National Science Foundation (CHE-0450085 and ECS-0901348), and the Houston Area Research Council.

BIOGRAPHICAL INFORMATION

K. F. Kelly received a B.S. in engineering physics from Colorado School of Mines in 1993 and a Ph.D. in applied physics from Rice University in 1999. He joined the ECE department in 2002 after postdoctoral fellowships at the Institute for Materials Research in Sendai, and in the chemistry department at Penn State University. His lab is currently focused on imaging and spectroscopy at the nanoscale along with understanding the role of mathematics in image acquisition and interpretation.

W. E. Billups obtained a B.S. in chemistry degree from Marshall University in 1961. After a period in industry, he entered the graduate program at the Pennsylvania State University where he received the Ph.D. in 1970. He then joined the Chemistry Department at Rice University. His current research interests are focused on the synthesis of soluble carbon nanomaterials.

FOOTNOTES

*To whom correspondence should be addressed. E-mail: billups@rice.edu.
The authors declare no competing financial interest.

REFERENCES

1 Berger, C.; Song, Z.; Li, T.; Li, X.; Ogbazghi, A. Y.; Feng, R.; Dai, Z.; Marchenkov, A. N.; Conrad, E. H.; First, P. N.; de Heer, W. A. Ultrathin epitaxial graphite: 2D electron gas properties and a route toward graphene-based nanoelectronics. *J. Phys. Chem. B* **2004**, *108*, 19912–19916.

2 Novoselov, K. S.; Geim, A. K.; Morozov, S. V.; Jiang, D.; Katsnelson, M. I.; Grigorieva, I. V.; Dubonos, S. V.; Firsov, A. A. Two-dimensional gas of massless Dirac fermions in graphene. *Nature* **2005**, *438*, 197–200.

3 Zhang, Y.; Tan, Y.-W.; Stormer, H. L.; Kim, P. Experimental observation of the quantum Hall effect and Berry's phase in graphene. *Nature* **2005**, *438*, 201–204.

4 Stankovich, S.; Dikin, D. A.; Dommett, G. H. B.; Kohlhaas, K. M.; Zimney, E. J.; Stach, E. A.; Piner, R. D.; Nguyen, S. T.; Ruoff, R. S. Graphene-based composite materials. *Nature* **2006**, *442*, 282–286.

5 Niyogi, S.; Bekyarova, E.; Itkis, M. E.; McWilliams, J. L.; Hamon, M. A.; Haddon, R. C. Solution properties of graphite and graphene. *J. Am. Chem. Soc.* **2006**, *128*, 7720–7721.

6 Han, M. Y.; Özyilmaz, B.; Zhang, Y.; Kim, P. Energy band-gap Engineering of Graphene Nanoribbons. *Phys. Rev. Lett.* **2007**, *98*, 206805.

7 Zhou, S. Y.; Gweon, G.-H.; Fedorov, A. V.; First, P. N.; de Heer, W. A.; Lee, D.-H.; Guinea, F.; Castro Neto, A. H.; Lanzara, A. Substrate-induced bandgap opening in epitaxial graphene. *Nat. Mater.* **2007**, *6*, 916.

8 Watcharotone, S.; Dikin, D. A.; Stankovich, S.; Piner, R.; Jung, I.; Dommett, G. H. B.; Evmenenko, G.; Wu, S.-E.; Chen, S.-F.; Liu, C.-P.; Nguyen, S. T.; Ruoff, R. S. Graphene-silica composite thin films as transparent conductors. *Nano Lett.* **2007**, *7*, 1888–1892.

9 Geim, A. K.; Novoselov, K. S. The rise of graphene. *Nat. Mater.* **2007**, *6*, 183–191.

10 Bunch, J. S.; van der Zande, A. M.; Verbridge, S. S.; Frank, I. W.; Tanenbaum, D. M.; Parpia, J. M.; Craighead, H. G.; McEuen, P. L. Electromechanical resonators from graphene sheets. *Science* **2007**, *315*, 490–493.

11 Pereira, J. M.; Vasilopoulos, P.; Peeters, F. M. Tunable quantum dots in bilayer graphene. *Nano Lett.* **2007**, *7*, 946–949.

12 Ramanathan, T.; Abdala, A. A.; Stankovich, S.; Dikin, D. A.; Herrera Alonso, M.; Piner, R. D.; Adamson, D. H.; Schniepp, H. C.; Chen, X.; Ruoff, R. S.; Nguyen, S. T.; Aksay, I. A.; Prud'Homme, R. K.; Brinson, L. C. Functionalized graphene sheets for polymer nanocomposites. *Nat. Nanotechnol.* **2008**, *3*, 327–331.

13 Stoller, M. D.; Park, S.; Zhu, Y.; An, J.; Ruoff, R. S. Graphene-based ultracapacitors. *Nano Lett.* **2008**, *8*, 3498–3502.

14 Freitag, M. Graphene: Nanoelectronics goes flat out. *Nat. Nanotechnol.* **2008**, *3*, 455–457.

15 Blake, P.; Brimicombe, P. D.; Nair, R. R.; Booth, T. J.; Jiang, D.; Schedin, F.; Ponomarenko, L. A.; Morozov, S. V.; Gleeson, H. F.; Hill, E. W.; Geim, A. K.; Novoselov, K. S. Graphene-based liquid crystal device. *Nano Lett.* **2008**, *8*, 1704–1708.

16 Hong, S.; Yoon, Y.; Guo, J. Metal-semiconductor junction of graphene nanoribbons. *Appl. Phys. Lett.* **2008**, *92*, 083107–083109.

17 Bolotin, K. I.; Sikes, K. J.; Jiang, Z.; Klima, M.; Fudenberg, G.; Hone, J.; Kim, P.; Stormer, H. L. Ultrahigh electron mobility in suspended graphene. *Solid State Commun.* **2008**, *146*, 351–355.

18 Lee, C.; Wei, X.; Kysar, J. W.; Hone, J. Measurement of the elastic properties and intrinsic strength of monolayer graphene. *Science* **2008**, *321*, 385–388.

19 Ghosh, S.; Calizo, I.; Teweldebrhan, D.; Pokatilov, E. P.; Nika, D. L.; Balandin, A. A.; Bao, W.; Miao, F.; Lau, C. N. Extremely high thermal conductivity of graphene: Prospects for thermal management applications in nanoelectronic circuits. *Appl. Phys. Lett.* **2008**, *92*, 151911.

20 Balandin, A. A.; Ghosh, S.; Bao, W.; Calizo, I.; Teweldebrhan, D.; Miao, F.; Lau, C. N. Superior thermal conductivity of single-layer graphene. *Nano Lett.* **2008**, *8*, 902–907.

21 Mak, K. F.; Sfeir, M. Y.; Wu, Y.; Lui, C. H.; Misewich, J. A.; Heinz, T. F. Measurement of the optical conductivity of graphene. *Phys. Rev. Lett.* **2008**, *101*, 196405.

22 Fowler, J. D.; Allen, M. J.; Tung, V. C.; Yang, Y.; Kaner, R. B.; Weiller, B. H. Practical chemical sensors from chemically derived graphene. *ACS Nano* **2009**, *3*, 301–306.

23 Sprinkle, M.; Ruan, M.; Hu, Y.; Hankinson, J.; Rubio Roy, M.; Zhang, B.; Wu, X.; Berger, C.; de Heer, W. A. Scalable templated growth of graphene nanoribbons on SiC. *Nat. Nanotechnol.* **2010**, *5*, 727–731.

24 Sun, Z.; Kohama, S.-i.; Zhang, Z.; Lomeda, J.; Tour, J. Soluble graphene through edge-selective functionalization. *Nano Res.* **2010**, *3*, 117–125.

25 Zacharia, R.; Ulbricht, H.; Hertel, T. Interlayer cohesive energy of graphite from thermal desorption of polyaromatic hydrocarbons. *Phys. Rev. B* **2004**, *69*, 155406.

26 Novoselov, K. S.; Geim, A. K.; Morozov, S. V.; Jiang, D.; Zhang, Y.; Dubonos, S. V.; Grigorieva, A. A. Electric Field Effect in Atomically Thin Carbon Films. *Science* **2004**, *306*, 666–669.

27 Stankovich, S.; Dikin, D. A.; Piner, R. D.; Kohlhaas, K. A.; Kleinhammes, A.; Jia, Y.; Wu, Y.; Nguyen, S. T.; Ruoff, R. S. Synthesis of graphene-based nanosheets via chemical reduction of exfoliated graphite oxide. *Carbon* **2007**, *45*, 1558–1565.

28 Li, D.; Müller, M. B.; Gilje, S.; Kaner, R. B.; Wallace, G. G. Processable aqueous dispersions of graphene nanosheets. *Nat. Nanotechnol.* **2008**, *3*, 101–105.

29 Tung, V. C.; Allen, M. J.; Yang, Y.; Kaner, R. B. High-throughput solution processing of large-scale graphene. *Nat. Nanotechnol.* **2009**, *4*, 25–29.

30 Vallés, C.; Drummond, C.; Saadaoui, H.; Furtado, C. A.; He, M.; Roubeau, O.; Ortolani, L.; Monthioux, M.; Pénicaud, A. Solutions of negatively charged graphene sheets and ribbons. *J. Am. Chem. Soc.* **2008**, *130*, 15802–15804.

31 Li, X.; Zhang, G.; Bai, X.; Sun, X.; Wang, X.; Wang, E.; Dai, H. Highly conducting graphene sheets and Langmuir-Blodgett films. *Nat. Nanotechnol.* **2008**, *3*, 538–542.

32 Behabtu, N.; Lomeda, J. R.; Green, M. J.; Higginbotham, A. L.; Sinitskii, A.; Kosynkin, D. V.; Tsentalovich, D.; Parra-Vasquez, A. N. G.; Schmidt, J.; Kesselman, E.; Cohen, Y.; Talmon, Y.; Tour, J. M.; Pasquali, M. Spontaneous high-concentration dispersions and liquid crystals of graphene. *Nat. Nanotechnol.* **2010**, *5*, 406–411.

33 Shih, C.-J.; Vijayaraghavan, A.; Krishnan, R.; Sharma, R.; Han, J.-H.; Ham, M.-H.; Jin, Z.; Lin, S.; Paulus, G. L.C.; Reuel, N. F.; Wang, Q. H.; Blankschtein, D.; Strano, M. S. Bi- and trilayer graphene solutions. *Nat. Nanotechnol.* **2011**, *6*, 439–445.

34 Dresselhaus, M. S.; Dresselhaus, G. Intercalation compounds of graphite. *Adv. Phys.* **2002**, *51*, 1–186.

35 Liang, F.; Sadana, A. K.; Peera, A.; Chattopadhyay, J.; Gu, Z.; Hauge, R. H.; Billups, W. E. A convenient route to functionalized carbon nanotubes. *Nano Lett.* **2004**, *4*, 1257–1260.

36 Chattopadhyay, J.; Mukherjee, A.; Chakraborty, S.; Kang, J.; Loos, P. J.; Kelly, K. F.; Schmidt, H. K.; Billups, W. E. Exfoliated soluble graphite. *Carbon* **2009**, *47*, 2945–2949.

37 Sun, Y.; Kuznetsov, O.; Alemany, L. B.; Billups, W. E. Reductive alkylation of anthracite: Edge functionalization. *Energy Fuels* **2011**, *25*, 3997–4005.

38 Stephenson, J. J.; Sadana, A. K.; Higginbotham, A. L.; Tour, J. M. Highly functionalized and soluble multiwalled carbon nanotubes by reductive alkylation and arylation: The Billups Reaction. *Chem. Mater.* **2006**, *18*, 4658–4661.

39 Zhao, S.; Zhao, X.; Fan, H.; Yang, L.; Zhang, Y.; Yang, J. Fabrication of graphene by cleaving graphite chemically. *Chem. Res. Chin. Univ.* **2011**, *27*, 547–549.

40 Lagow, R. J.; Badachhape, R. B.; Wood, J. L.; Margrave, J. L. Some new synthetic approaches to graphite-fluorine chemistry. *J. Chem. Soc., Dalton Trans.* **1974**, *12*, 1268–1273.

41 Rüdorff, W.; Rüdorff, G. Zur konstitution des kohlenstoff-monofluorids. *Z. Anorg. Chem.* **1947**, *253*, 281–296.

42 Worsley, K. A.; Ramesh, P.; Mandal, S. K.; Niyogi, S.; Itkis, M. E.; Haddon, R. C. Soluble graphene derived from graphite fluoride. *Chem. Phys. Lett.* **2007**, *445*, 51–53.

43 Chakraborty, S.; Guo, W.; Hauge, R. H.; Billups, W. E. Reductive alkylation of fluorinated graphite. *Chem. Mater.* **2008**, *20*, 3134–3136.

44 Saini, R. K.; Chiang, I. W.; Peng, H.; Smalley, R. E.; Billups, W. E.; Hauge, R. H.; Margrave, J. L. Covalent sidewall functionalization of single wall carbon nanotubes. *J. Am. Chem. Soc.* **2003**, *125*, 3617–3621.

45 Chamssedine, F.; Dubois, M.; Guérin, K.; Giraudet, J.; Masin, F.; Ivanov, D. A.; Vidal, L.; Yazami, R.; Hamwi, A. Reactivity of carbon nanofibers with fluorine gas. *Chem. Mater.* **2007**, *19*, 161–172.

46 Reghai, L.; Conard, J.; Fuzellier, H.; Lelaurain, M.; McRae, E. Transport and ^{13}C nuclear magnetic resonance studies on potassium,ammonia intercalated graphite. *J. Phys. Chem. Solids* **2001**, *62*, 2083–2090.

47 Whangbo, M.-H.; Liang, W.; Ren, J.; Magonov, S. N.; Wawkuschewski, A. Structural and electronic properties of graphite and graphite intercalation compounds MC_8 (M = K, Rb, Cs) governing their scanning tunneling microscopy images. *J. Phys. Chem.* **1994**, *98*, 7602–7606.

48 Estrade-Szwarckopf, H.; Rousseau, B. U.P.S. and X.P.S. studies of alkali-graphite intercalation compounds. *Synth. Met.* **1988**, *23*, 191–198.

49 Okabe, K.; Tanuma, S. Dynamics of stage boundaries in alkali-metal GICs observed by color photography. *Synth. Met.* **1988**, *23*, 61–66.

50 Braga, D.; Ripamonti, A.; Savoia, D.; Trombini, C.; Umani-Ronchi, A. Graphite lamellar compounds. A new route to transition metal intercalates. *J. Chem. Soc., Chem. Commun.* **1978**, 927–928.

51 Haworth, D. T.; Wilkie, C. A. The solid state ^{13}C-NMR spectra of some intercalation compounds. *J. Solid State Chem.* **1980**, *31*, 343–345.

52 Nixon, D. E.; Parry, G. S. Formation and structure of the potassium graphites. *J. Phys. D: Appl. Phys.* **1968**, *1*, 291–298.

53 Chakraborty, S.; Chattopadhyay, J.; Guo, W.; Billups, W. E. Functionalization of potassium graphite. *Angew. Chem., Int. Ed.* **2007**, *46*, 4486–4488.

54 Boersma, M. A. M. Catalytic properties of alkalimetal-graphite intercalation compounds. *Catal. Rev.* **1974**, *10* (55), 243–280.

55 Sierra, M. A.; Ramírez-López, P.; Gómez-Gallego, M.; Lejon, T.; Mancheño, M. J. C_8K-Promoted self-condensation and self-condensation-cycloisomerization reactions of α,β-unsaturated fischer carbene complexes. *Angew. Chem.* **2002**, *114*, 3592–3595; *Angew. Chem., Int. Ed.* **2002**, *41*, 3442–3445.

56 Weitz, I. S.; Rabinovitz, M. The application of C_8K for organic synthesis: reduction of substituted naphthalenes. *J. Chem. Soc., Perkin Trans. 1* **1993**, 117–120.

57 Fürstner, A.; Weidmann, H. Highly selective metal-graphite-induced reductions of deoxy halo sugars. *J. Org. Chem.* **1989**, *54*, 2307–2311.

58 Fürstner, A.; Weidmann, H. Efficient formation and cleavage of disilanes by potassium-graphite. Silylation with silyl metal reagents. *J. Organomet. Chem.* **1988**, *354*, 15–21.

59 Mindiola, D. J.; Hillhouse, G. L. Terminal amido and imido complexes of three-coordinate nickel. *J. Am. Chem. Soc.* **2001**, *123*, 4623–4624.

60 Schwindt, M. A.; Lejon, T.; Hegedus, L. S. Improved synthesis of (aminocarbene)-chromium(0) complexes with use of C_8K-generated $Cr(CO)_5^{2-}$. Multivariant optimization of an organometallic reaction. *Organometallics* **1990**, *9*, 2814–2819.

61 Fürstner, A. Metal-graphite reagents in carbohydrate chemistry, IX fragmentations of 1-deoxy-1-iodo-2,3;4,5-di-O-isopropylidene pentitols. *Tetrahedron Lett.* **1990**, *31*, 3735–3738.

62 Fürstner, A.; Weidmann, H. A simple and efficient new glycal synthesis. *J. Carbohydr. Chem.* **1988**, *7*, 773–783.

63 Contento, M.; Savoia, D.; Trombini, C.; Umani-Ronchi, A. Potassium-graphite as selective reducing agent for activated double bond systems. *Synthesis* **1979**, 30–32.

64 Ungurenasu, C.; Palie, M. Reactions of C_8K with metal carbonyls. *J. Chem. Soc., Chem. Commun.* **1975**, 388.

65 Jensen, K. A.; Nygaard, B.; Glisson, G.; Nielson, P. H. Reductions with potassium eraphitate. I. Preparation of nickel(0) complexes of trialkyl phosphites. *Acta Chem. Scand.* **1965**, *19*, 768–770.

66 Savoia, D.; Trombini, C.; Umani-Ronchi, A. Potassium-graphite (C8K) as a metallation reagent. Alkylation of nitriles and esters with alkyl halides under heterogeneous conditions. *Tetrahedron Lett.* **1977**, *18*, 653–656.

67 Savoia, D.; Trombini, C.; Umani-Ronchi, A. Potassium-graphite as a metalation reagent. Synthesis of aldehydes and ketones by alkylation of imines and dihydro-1,3-oxazine. *J. Org. Chem.* **1978**, *43*, 2907–2910.

68 Savoia, D.; Trombini, C.; Umani-Ronchi, A. Selective alkylation of allyl phenyl Sulphone. A novel synthesis of alk-2-enes. *J. Chem. Soc., Perkin Trans. 1* **1977**, 123–125.

69 Ellingsen, P. O.; Undeheim, K. Sulfones in Horner-Witting synthesis of alkenes. *Acta Chem. Scand., Ser. B* **1979**, *33*, 528–530.

70 Bergbreiter, D. E.; Killough, J. M. Lewis base properties of potassium-graphite. *J. Chem. Soc., Chem. Commun.* **1976**, 913–914.

71 Bergbreiter, D. E.; Killough, J. M. Reactions of potassium-graphite. *J. Am. Chem. Soc.* **1978**, *100*, 2126–2134.

72 Rabinovitz, M.; Tamarkin, D. Facile Debromination by potassium-graphite intercalate. *Synth. Commun.* **1984**, *14*, 377–379.

73 Rabinovitz, M.; Tamarkin, D. Graphite-potassium intercalate - C_8K - an efficient agent for ring closure reactions. *Synth. Met.* **1988**, *23*, 487–491.

74 Setton, R.; Beguin, F.; Piroelle, S. Graphite intercalation compounds as reagents in organic synthesis. An overview and some recent applications. *Synth. Met.* **1982**, *4*, 299–318.

75 Ebert, L. B. Is soot composed predominantly of carbon clusters? *Science* **1990**, *247*, 1468–1471.

76 Liang, F.; Alemany, L. B.; Beach, J. M.; Billups, W. E. Structure Analyses of Dodecylated Single-Walled Carbon Nanotubes. *J. Am. Chem. Soc.* **2005**, *127*, 13941–13948.

77 Sadana, A. K.; Liang, F.; Brinson, B.; Arepalli, S.; Farhat, S.; Hauge, R. H.; Smalley, R. E.; Billups, W. E. Functionalization and extraction of large fullerenes and carbon-coated metal formed during the synthesis of single wall carbon nanotubes by laser oven, direct current arc, and high-pressure carbon monoxide production methods. *J. Phys. Chem. B* **2005**, *109*, 4416–4418.

78 Chattopadhyay, J.; de Jesus Cortez, F.; Chakraborty, S.; Slater, N. K. H.; Billups, W. E. Synthesis of water-soluble pegylated single-walled carbon nanotubes. *Chem. Mater.* **2006**, *18*, 5864–5868.

79 Buseck, P. R.; Huang, B.; Keller, L. P. Electron microscope investigation of the structures of annealed carbons. *Energy Fuels* **1987**, *1*, 105–110.

80 Mukherjee, A.; Kang, J.; Kuznetsov, O.; Sun, Y.; Thaner, R.; Bratt, A. S.; Lomeda, J. R.; Kelly, K. F.; Billups, W. E. Water-soluble graphite nanoplatelets formed by oleum exfoliation of graphite. *Chem. Mater.* **2011**, *23*, 9–13.

81 Liang, F.; Beach, J. M.; Rai, P. K.; Guo, W.; Hauge, R. H.; Pasquali, M.; Smalley, R. E.; Billups, W. E. Highly exfoliated water-soluble single-walled carbon nanotubes. *Chem. Mater.* **2006**, *18*, 1520–1524.

82 Ferrari, A. C.; Meyer, J. C.; Scardaci, V.; Casiraghi, C.; Lazzeri, M.; Mauri, F.; Piscanec, S.; Jiang, D.; Novoselov, K. S.; Roth, S.; Geim, A. K. Raman spectrum of graphene and graphene layers. *Phys. Rev. Lett.* **2006**, *97*, 187401–187404.

83 Ferrari, A. C. Raman spectroscopy of graphene and graphite: Disorder, electron-phonon coupling, doping and nonadiabatic effects. *Solid State Commun.* **2007**, *143*, 47–57.

84 Kelly, K. F.; Mickelson, E. T.; Hauge, R. H.; Margrave, J. L.; Halas, N. J. Nanoscale imaging of chemical interactions: Fluorine on graphite. *Proc. Natl. Acad. Sci. U.S.A.* **2000**, *97*, 10318–10321.

85 Wang, X.; Zhi, L.; Mullen, K. Transparent, conductive graphene electrodes for dye-sensitized solar cells. *Nano Lett.* **2007**, *8*, 323–327.

86 Kim, K. S.; Zhao, Y.; Jang, H.; Lee, S. Y.; Kim, J. M.; Kim, K. S.; Ahn, J.-H.; Kim, P.; Choi, J.-Y.; Hong, B. H. Large-scale pattern growth of graphene films for stretchable transparent electrodes. *Nature* **2009**, *457*, 706–710.